is *not* stabilized by bridging ligands.[12-15] The molecular structure of this complex is unique. In addition, the rather large "empty" cavity within the central ring of the molecule (of area approximately 21 Å^2) possesses dimensions appropriate for the insertion of small molecules. There is much potential for binuclear catalytic activity.

The complex [ZnBr([12]aneN$_3$)]Br is mononuclear with a slightly distorted tetrahedral coordination environment about zinc. Our data indicate that the macrocycle [12]aneN$_3$ is sufficiently flexible to conform to the normal coordination requirements of the zinc(II) ion and does not have the same rigid steric requirements as the smaller symmetrical triaza species, [9]aneN$_3$.[2,7,8,50,51]

Addendum. A reviewer drew our attention to a communication by Margulis and Zompa[52] in which the synthesis of [20]aneN$_6$ (as a byproduct of synthesizing [10]aneN$_3$) is reported along with a structural study of the mononuclear nickel(II) complex [Ni([20]aneN$_6$)][ClO$_4$]$_2$·DMF.

Acknowledgment. We thank Professor R. D. Bereman and P. J. Hochgesang (North Carolina State University) and Professor R. D. Allendoerfer (University at Buffalo, SUNY) for their assistance in obtaining ESR spectra.

Registry No. **2**·6HBr, 113380-64-6; [ZnBr(**1**)]Br, 113380-63-5; Cu$_2$(**2**)Br$_4$, 113380-62-4.

Supplementary Material Available: Tables S1 and S2, listing hydrogen atom coordinates and anisotropic thermal parameters for Cu$_2$([24]aneN$_6$)Br$_4$, and Tables S3 and S4, with similar information for [ZnBr([12]aneN$_3$)]Br (5 pages); tables of calculated and observed structure factor amplitudes (21 pages). Ordering information is given on any current masthead page.

(50) Schwindinger, W. F.; Fawcett, T. G.; Lalancette, R. A.; Potenza, J. A.; Schugar, H. J. *Inorg. Chem.* **1980**, *19*, 1379.
(51) Wieghardt, K.; Guttmann, M.; Chaudhuri, P.; Gebert, W.; Minelli, M.; Young, C. G.; Enemark, J. H. *Inorg. Chem.* **1985**, *24*, 3151.
(52) Margulis, T. N.; Zompa, L. J. *J. Chem. Soc., Chem. Commun.* **1979**, 430.

Contribution from the Corporate Research-Science Laboratories, Exxon Research and Engineering Company, Annandale, New Jersey 08801

Structure and Magnetic Properties of $V_2(VO)(P_2O_7)_2$. A Mixed-Valence Vanadium(III,III,IV) Pyrophosphate

Jack W. Johnson,* David C. Johnston,*† Hubert E. King, Jr., Thomas R. Halbert, John F. Brody, and David P. Goshorn

Received November 20, 1987

A new pyrophosphate of mixed-valent vanadium, $V_2(VO)(P_2O_7)_2$, has been synthesized by the reaction of $VO(PO_3)_2$ with VPO_4. Single crystals were formed as a minor phase during high-temperature annealing of $(VO)_2P_2O_7$. The new compound is orthorhombic, space group *Pnma*, with a = 17.459 (3) Å, b = 12.185 (2) Å, c = 5.2431 (7) Å, V = 1115.4 (3) Å^3, and Z = 4. The structure was determined by single-crystal X-ray diffraction with final residuals R = 0.0350 and R_w = 0.0339. $V_2(VO)(P_2O_7)_2$ consists of linear vanadium trimers containing two octahedrally coordinated V^{3+} cations joined through edges to a central V^{4+} square pyramid. These trimers are linked in three dimensions through the pyrophosphate groups. The magnetic susceptibility, measured from 1 to 300 K, shows that the vanadium(III) ions in the trimer are antiferromagnetically coupled to the central vanadium(IV) ion with J = −22 cm^{-1}. Longer range interactions lead to bulk antiferromagnetic order below 5 K.

Introduction

Vanadyl(IV) pyrophosphate, $(VO)_2P_2O_7$, has been the subject of recent studies due to its efficacy as catalyst for the oxidation of butane to maleic anhydride as well as for its interesting magnetic properties. Ladders of antiferromagnetically coupled V^{4+} ions run throughout the structure, giving rise to magnetic behavior similar to that of linear-chain compounds.[1] In order to study the antiferromagnetic ordering in more detail at temperatures below 4 K, better crystals than those available by prior techniques were needed to minimize the effect of paramagnetic defects. While attempting to grow crystals of $(VO)_2P_2O_7$ from the melt at 1000 °C, we observed formation of a minor phase by X-ray powder diffraction. Single-crystal analysis of a few small well-formed crystals gave unit cell constants that did not correspond to any known phase of vanadium phosphate, so a structure determination was undertaken. Successful solution of the structure showed that a new phase of vanadium phosphate had been formed with a formula $V_3P_4O_{15}$.

The structure consists of vanadium trimers composed of two trivalent vanadium atoms and one tetravalent vanadyl group. The trimers are linked together by $P_2O_7^{4-}$ groups. The compound can be synthesized in bulk microcrystalline form by the reaction of $VO(PO_3)_2$ with VPO_4. Investigation of the magnetic susceptibility shows that the V^{3+} ions are antiferromagnetically coupled to the V^{4+} ion and that intertrimer interactions lead to antiferromagnetic ordering below 5 K.

Experimental Section

Materials. $(VO)_2P_2O_7$ was prepared by heating $VO(HPO_4)\cdot 0.5H_2O$ for 20 h at 700 °C in flowing helium.[2] VPO_4 was prepared by decomposition of $(NH_4)_2[(VO)_2(HPO_4)_2(C_2O_4)]\cdot 5H_2O$ at 980 °C.[3] $VO(PO_3)_2$ was prepared by dehydration of $VO(H_2PO_4)_2$ at 700 °C under flowing helium.[4]

Preparation of $V_3P_4O_{15}$. A sample of $(VO)_2P_2O_7$ was placed in a crimped platinum tube, which was sealed in an evacuated silica tube, heated to 1030 °C to melt the charge, and slowly cooled to 800 °C. Upon air quenching and examination of the crystalline product by X-ray powder diffraction, it was apparent that, in addition to $(VO)_2P_2O_7$, a small amount of an additional phase was present. A single-crystal diffraction study showed this second phase to be the new compound $V_3P_4O_{15}$. Subsequently, this new compound was prepared in pure form by reaction of VPO_4 and $VO(PO_3)_2$ in a 2:1 molar ratio at 850 °C for 4 days in an evacuated silica tube. The observed X-ray powder diffraction pattern corresponded well with that calculated from the single crystal data.

Magnetic susceptibility $\chi(T)$ data were obtained in a magnetic field H = 6.3 kG by using a George Associates Faraday magnetometer and sweeping the temperature at less than 1 K/min. The contribution of

† Present address: Department of Physics, Iowa State University, Ames, IA 50011.

(1) Johnston, D. C.; Johnson, J. W.; Goshorn, D. P.; Jacobson, A. J. *Phys. Rev. B: Condens. Matter* **1987**, *35*, 219-222.
(2) Johnson, J. W.; Johnston, D. C.; Jacobson, A. J.; Brody, J. F. *J. Am. Chem. Soc.* **1984**, *106*, 8123-8128.
(3) Ladwig, G.; Jost, K.-H.; Schlesinger, K. *Z. Chem.* **1978**, *19*, 386.
(4) Ladwig, G. *Z. Chem.* **1968**, *8*, 307-308.

0020-1669/88/1327-1646$01.50/0

Table I. Atomic Coordinates ($\times 10^4$) for $V_2(VO)(P_2O_7)_2$

atom	x/a	y/b	z/c	10^4U(iso), Å^2	B, Å^2
V(1)	1716 (1)	2500	4876 (4)	89 (5)	0.70
V(2)	1242.9 (7)	220 (1)	2437 (3)	76 (4)	0.60
P(1)	360 (1)	1323 (2)	7629 (5)	79 (5)	0.62
P(2)	3061 (1)	1254 (2)	2333 (5)	74 (5)	0.58
O(1)	3427 (3)	703 (4)	4559 (11)	172 (14)	1.36
O(2)	935 (3)	1314 (4)	5346 (10)	98 (13)	0.77
O(3)	2169 (3)	1326 (4)	2673 (11)	94 (12)	0.74
O(4)	798 (3)	1285 (5)	106 (11)	126 (14)	0.99
O(5)	3249 (3)	751 (4)	9803 (11)	152 (13)	1.20
O(6)	4742 (3)	502 (4)	7735 (11)	115 (13)	0.91
O(7)	4961 (4)	2500	7534 (16)	77 (16)	0.61
O(8)	2204 (4)	2500	7361 (19)	167 (19)	1.32
O(9)	3344 (4)	2500	2302 (17)	135 (18)	1.07

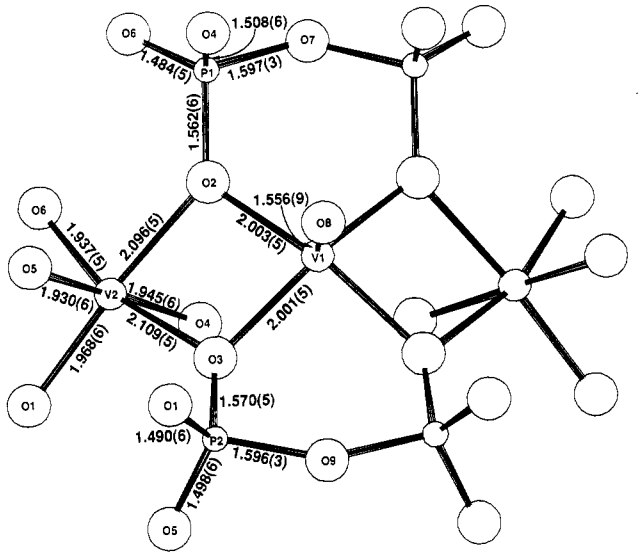

Figure 1. Structure of $V_2(VO)(P_2O_7)_2$, showing the trimeric vanadium unit, the atom labeling, and the important bond distances.

ferromagnetic impurities to the measured magnetization M was determined from $M(H)$ isotherms at several temperatures and was small, corresponding to ~30 atomic ppm of iron metal with respect to vanadium. The data presented are corrected for this contribution. Additional $\chi(T)$ data in H = 10 kG and $M(H)$ isotherms up to H = 65 kG were obtained by using a PAR vibrating sample magnetometer.

Structure Determination. A small, green, prismatic crystal having dimensions of approximately 0.15 × 0.05 × 0.05 mm^3 was mounted and placed on a Huber four-circle diffractometer equipped with graphite-monochromatized Mo Kα radiation, λ = 0.71069 Å, operating at 26 °C. Trial indexing, axial rotation photographs, and least-squares analysis of the setting angles for thirteen centered reflections led to an orthorhombic cell with a = 17.459 (3), b = 12.185 (2), and c = 5.2431 (7) Å, where one esd is indicated in parentheses. The structure was solved and refined by using integrated intensities measured for those reflections having $hkl \geq 0$ in the range $2° < 2\theta < 45°$. The 987 reflections, which included two reference reflections taken every 25 data, were measured by using a θ–2θ scan with backgrounds taken both before and after the scan. The reference reflections did not vary significantly over the course of data collection. Systematic absences in the resulting data indicated the diffraction symbol of Pn^*a. The centrosymmetric space group $Pnma$ was chosen for the subsequent structure solution and refinement. The data were corrected for Lorentz and polarization effects, and those data having $I < 3\sigma(I)$ were eliminated. Owing to the crystal's regular shape, small dimensions, and relatively small absorption coefficient, μ = 9.89 cm^{-1}, no absorption correction was applied. The resulting 563 symmetry-distinct structure factors were used to solve the structure by using the MULTAN portion of the Structure Determination Package (Enraf-Nonius, Delft, Holland). The model parameters were then refined through full-matrix least-squares techniques using the computer program CRYSTALS (Chemical Crystallography Laboratory, Oxford University). The final model included variable atom positions, isotropic thermal parameters, an extinction coefficient, and a scale factor. The conventional crystallographic residuals are R = 0.0350 and R_w = 0.0339 ($1/\sigma_F$ weights), with a data to parameter ratio of 563/50. The atomic coordinates for this model are given in Table I. The bond distances, bond angles, and errors calculated from these coordinates are given in Table II. A table of the observed and calculated structure factors is available as supplementary material.

Table II. Interatomic Distances (Å) and Angles (deg) in $V_2(VO)(P_2O_7)_2$

V(1)–V(2)	3.169 (2)	P(1)–O(2)	1.562 (6)
V(1)–O(2)	2.003 (5)	P(1)–O(4)	1.508 (6)
V(1)–O(3)	2.001 (5)	P(1)–O(6)	1.484 (5)
V(1)–O(8)	1.556 (9)	P(1)–O(7)	1.597 (3)
V(2)–O(1)	1.968 (6)	P(2)–O(1)	1.490 (6)
V(2)–O(2)	2.096 (5)	P(2)–O(3)	1.570 (5)
V(2)–O(3)	2.109 (5)	P(2)–O(5)	1.498 (6)
V(2)–O(4)	1.945 (6)	P(2)–O(9)	1.596 (3)
V(2)–O(5)	1.930 (6)		
V(2)–O(6)	1.937 (5)		
O(2)–V(1)–O(2)	92.4 (3)	O(3)–V(1)–O(2)	79.9 (2)
O(3)–V(1)–O(2)	148.8 (2)	O(3)–V(1)–O(3)	91.3 (3)
O(8)–V(1)–O(2)	105.7 (3)	O(8)–V(1)–O(3)	105.5 (3)
O(2)–V(2)–O(1)	175.2 (2)	O(3)–V(2)–O(1)	100.7 (2)
O(3)–V(2)–O(2)	75.4 (2)	O(4)–V(2)–O(1)	90.9 (2)
O(4)–V(2)–O(2)	86.0 (2)	O(4)–V(2)–O(3)	85.2 (2)
O(5)–V(2)–O(1)	90.5 (2)	O(5)–V(2)–O(2)	92.3 (2)
O(5)–V(2)–O(3)	90.1 (2)	O(5)–V(2)–O(4)	175.3 (2)
O(6)–V(2)–O(1)	93.6 (2)	O(6)–V(2)–O(2)	90.1 (2)
O(6)–V(2)–O(3)	165.0 (2)	O(6)–V(2)–O(4)	89.9 (2)
O(6)–V(2)–O(5)	94.4 (2)		
O(4)–P(1)–O(2)	109.6 (3)	O(6)–P(1)–O(2)	111.3 (3)
O(6)–P(1)–O(4)	117.3 (3)	O(7)–P(1)–O(2)	104.2 (4)
O(7)–P(1)–O(4)	107.2 (4)	O(7)–P(1)–O(6)	106.3 (3)
O(3)–P(2)–O(1)	111.2 (3)	O(5)–P(2)–O(1)	114.6 (3)
O(5)–P(2)–O(3)	109.9 (3)	O(9)–P(2)–O(1)	107.7 (4)
O(9)–P(2)–O(3)	104.8 (3)	O(9)–P(2)–O(5)	108.2 (4)
P(1)–O(7)–P(1)	127.8 (4)	P(2)–O(9)–P(2)	144.0 (5)

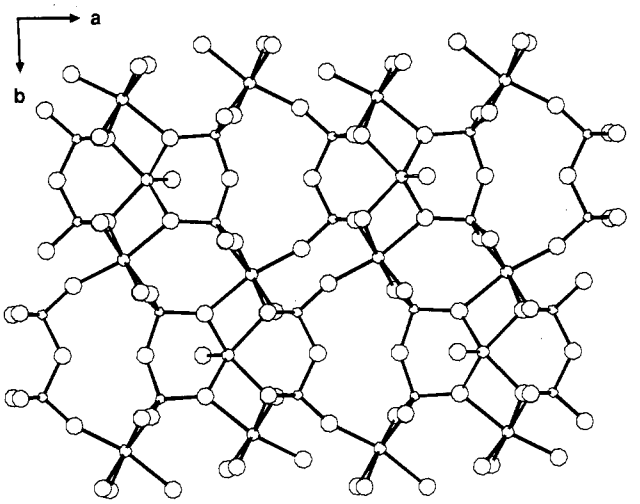

Figure 2. Structure of $V_2(VO)(P_2O_7)_2$ viewed down the crystallographic c axis. The small four-coordinate circles represent phosphorus atoms, the intermediate-sized five- and six-coordinate circles represent vanadium atoms, and the larger circles represent oxygen atoms.

Results and Discussion

Description of the Structure of $V_2(VO)(P_2O_7)_2$. The fundamental structural unit of $V_2(VO)(P_2O_7)_2$ is shown in Figure 1. It consists of a vanadium(IV) ion residing on a mirror plane coordinated by five oxygen atoms in a square pyramid. The unshared terminal oxygen atom (O(8)) is also on the mirror plane. Chelating pyrophosphate groups, bisected by the mirror plane at O(7), bridge opposing basal edges of the V^{4+} square pyramid. The remaining edges of the square pyramid are shared with the vanadium(III) octahedra, resulting in a linear vanadium trimer. The V^{3+}–V^{4+} distance within the trimer is 3.169 (2) Å, very similar to the V^{4+}–V^{4+} distance of 3.19 (1) Å found in $(VO)_2P_2O_7$, which contains vanadium(IV) in edge-sharing pairs of octahedra.[5] The structure is built up of these trimers linked together in three

(5) Gorbunova, Yu. E.; Linde, S. A. *Dokl. Akad. Nauk SSSR* **1979**, *245*, 584–588.

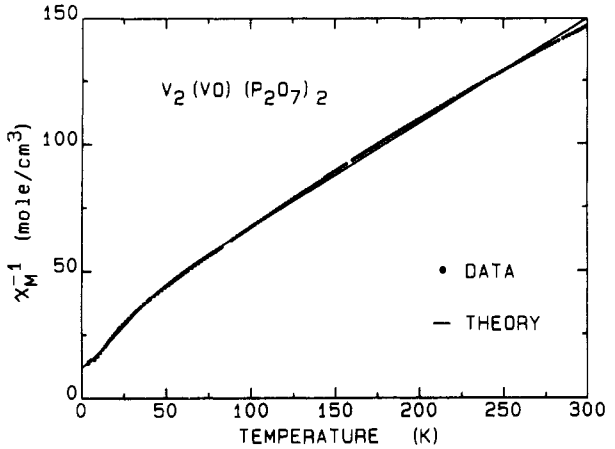

Figure 3. Inverse molar magnetic susceptibility (χ_m^{-1}) vs temperature for $V_2(VO)(P_2O_7)_2$ (solid dots), obtained by using the Faraday method. The solid curve is a theoretical fit to the data (see text).

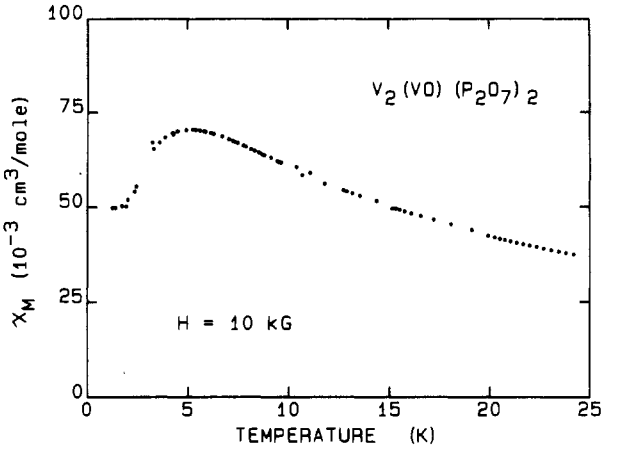

Figure 4. Magnetic susceptibility (χ_m) vs temperature obtained by using a vibrating sample magnetometer, illustrating antiferromagnetic ordering below 5 K.

dimensions by P–O-V bonds. A view down the *c* axis is presented in Figure 2. There are oxygen atoms with three different coordination numbers. The terminal oxygen atom O(8) forms the vanadyl(IV)–oxygen double bond and has a coordination number of one. Oxygen atoms O(2) and O(3) form the bridging edges and have a coordination number of three. The remainder of the oxygen atoms link the octahedral vanadium atoms to pyrophosphate groups of different trimers and have a coordination number of two. As can be seen from Figure 2, the structure is linked through P–O–V–O–P bonds in the *a* and *c* directions and through V–O–V–O–P–O–P–O–V linkages along *b*. The bond distances and angles around both vanadium and phosphorus are well within the expected ranges as shown in Table II and Figure 1. The deviation of the angles from the ideal can be explained by a displacement of V(2) from the center of its octahedron away from V(1) due to cation–cation repulsion. Within the phosphorus tetrahedra, the phosphorus–oxygen bond distances are longest for the P–O–P bonds, intermediate for the bonds to the three-coordinate O(2) and O(3) atoms, and shorter for the bonds to the two-coordinate O(1), O(5), O(4), and O(6) atoms.

Magnetic Properties. The inverse molar magnetic susceptibility χ_m^{-1} of $V_2(VO)(P_2O_7)$ is plotted versus temperature in Figure 3 (Faraday magnetometer data). The data are distinctly nonlinear, particularly below 100 K. At high temperatures, greater than 100 K, the data approach Curie–Weiss behavior, $\chi_m = C/(T - \Theta)$, with Curie constant $C = 2.5$ cm^3 K/mol and paramagnetic Curie temperature $\Theta = -71$ K. The value of C is close to that (2.38 cm^3 K/mol) expected for 2 mol of isolated V^{3+} ($S = 1$) and 1 mol of isolated V^{4+} ($S = {}^1/_2$) with the Lande *g* factor $g = 2$. Thus, the magnetic interactions responsible for the deviation of the data from the Curie law $\chi(M) = C/T$ are of magnitude <100 K and are antiferromagnetic ($\Theta < 0$).

In order to model the data in Figure 3, we assume that the two V^{3+} ions within a trimer interact with the V^{4+} central ion via the Heisenberg interaction, but do not interact with each other. The intratrimer Hamiltonian is then

$$\mathbf{H} = -2J(\vec{S}_1 + \vec{S}_2)\cdot\vec{S}_3 \qquad (1)$$

where $S_1 = S_2 = 1$ are the V^{3+} spins and $S_3 = {}^1/_2$ is the V^{4+} spin. Equation 1 is easily diagonalized, yielding the energy eigenvalues $E_S = 0$ ($S = {}^1/_2$), $2J$ ($S = {}^1/_2$), $-J$ ($S = {}^3/_2$), $3J$ ($S = {}^3/_2$), and $-2J$ ($S = {}^5/_2$) for the states of the trimer with total spin S. The magnetic susceptibility is then

$$\chi_m(T) = \frac{N_A g^2 \mu_B^2 \sum_S S(S+1)(2S+1)\exp(-E_S/k_BT)}{3k_BT\sum_S (2S+1)\exp(-E_S/k_BT)} \qquad (2)$$

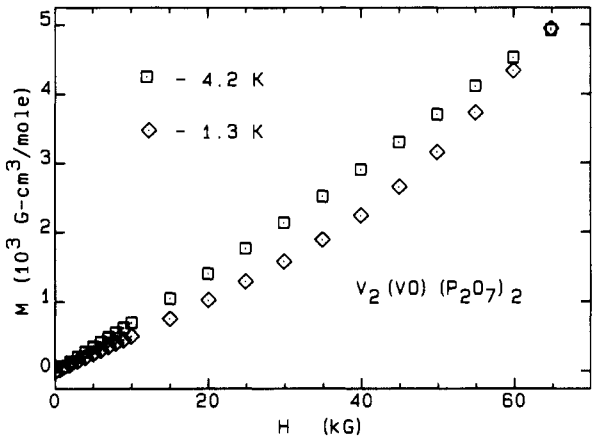

Figure 5. Magnetization (M) vs the applied magnetic field (H) isotherms at 1.3 and 4.2 K.

where N_A is Avogadro's number, μ_B is the Bohr magneton, and k_B is Boltzmann's constant. Intertrimer interactions, necessary because of the occurrence of antiferromagnetic ordering below 5 K (see below), are incorporated into our model in a mean field way by replacing T in (2) by $(T - \Theta)$, where Θ is a measure of the sign and magnitude of these interactions. A nonlinear least-squares fit of (2) to the data in Figure 3 is shown as the solid curve in the figure. The fitting parameters were found to be physically reasonable: $g = 1.99$, $J/k_B = -32$ K (antiferromagnetic), and $\Theta = -22$ K (antiferromagnetic).

The magnetic susceptibility from 1 to 25 K in a field of 10 kG obtained by using the vibrating sample magnetometer is shown in Figure 4. As in Figure 3, $\chi_m(T)$ increases with decreasing T down to ~5 K, but then reaches a maximum value χ_m^{max} and decreases to $\sim 2/3\ \chi_m^{max}$ as $T \to 0$. This is the signature of long-range antiferromagnetic ordering at $T_N \sim 5$ K. This interpretation is supported by $M(H)$ isotherm data up to $H = 65$ kG shown in Figure 5 for $T = 1.3$ and 4.2 K. The positive curvature in $M(H)$, which is quite pronounced in the data obtained at 1.3 K, is indicative of a "spin-flop" transition with an onset at about 39 kG. This transition is caused by a reorientation of the spins in an antiferromagnetically ordered sample to a direction perpendicular to the applied magnetic field.

Registry No. $V_3P_4O_{15}$, 113668-26-1.

Supplementary Material Available: A table of observed and calculated structure factors (6 pages). Ordering information is given on any current masthead page.